ADVANCED MATERIALS

COMMUNICATION

DOI: 10.1002/adma.200702999

Enhanced Optical Properties of a Photosynthetic System Conjugated with Semiconductor Nanoparticles: The Role of Förster Transfer[**]

By *Alexander O. Govorov**

Modern nanobiotechnology offers the possibility to combine crystalline nanoparticles (NPs) and biomolecules in one superstructure, refereed to as a bioconjugate.[1,2] Owing to interactions between nanocrystals and molecules, bioconjugates acquire novel properties that can be utilized for energy conversion,[3,4] optical imaging, and sensing.[5,6] In semiconductor-NP–dye conjugates, for instance, the exciton energy can be transferred from a NP to a dye molecule via Förster transfer (FT). Since a biolinker between a dye molecule and a NP can be made sensitive to a chemical composition of a solution, temperature, or pH, the efficiency of the Förster transfer can be used for biodetection and bioimaging.[5,6] Another type of interaction present in dye–metal-NP complexes appears because of to exciton–plasmon coupling.[7–9] In his case, plasmon excitations in a metal NP that lead to amplification of electromagnetic fields in the vicinity of a molecule can strongly alter optical emission from attached dye molecules. Optical emission of dye molecules can be enhanced or suppressed, depending on the dye–NP distance. Along with dye molecules, current research involves photosynthesis systems.[3,4,10] The key function of the photosynthesis systems is to harvest sunlight energy and transfer the excitation for rapid charge separation of optically generated electron–hole pairs. If a metal NP is conjugated with a photosynthetic system, the plasmon enhancement effect can lead to a strongly increased rate of production of excited electrons that can be used for photocurrents or for chemical reactions.[11] In very recent experiments, single chlorophylls containing light-harvesting complexes have been placed in the vicinity of silver nanocrystals and exhibited strong plasmon-assisted enhancement of fluorescence, indicating a strongly increased rate of generation of excitations in the chlorophylls.[12]

Here we propose and model a hybrid complex composed of a photosystem (PS) and semiconductor NP. We show that the rate of optical generation of electron–hole pairs inside a photosynthetic system can be greatly increased through conjugation with semiconductor nanoparticles. The enhancement effect comes from the much larger optical absorption cross-section of a semiconductor nanoparticle compared to a photosynthetic system. Under realistic conditions, the enhancement factor can be as high as 100. In the hybrid complex, excitons are optically generated in a semiconductor nanoparticle and transferred via the Förster mechanism to the photosynthetic system, where charge separation takes place. The excited electrons can be utilized for chemical transformations or for generating photocurrents. In contrast to natural photosynthetic systems, which absorb solar energy only within certain wavelength intervals, the proposed hybrid structure is able to absorb sunlight in a much broader spectral range. Because of radiative losses of a nanoparticle, the quantum yield of a hybrid structure is reduced. The hybrid system, modeled and proposed here, can be used for light-harvesting applications.

Strong enhancement of opto-electronic properties of the PS–NP complex comes from the unique combination of properties of the building blocks. The semiconductor NP strongly absorbs light and, on the other hand, the photosystem efficiently separates electrons and holes. It is also important to compare this hybrid system with the structure proposed in our previous paper[11] and realized in a recent experiment.[12] The structure described in Ref. [11] incorporated a metal NP and PS. In such a complex, the mechanism of enhancement is due to the plasmon resonance whereas, in the semiconductor-NP–PS complex studied here, the key interaction comes from Förster energy transfer. In fact, Förster transfer in the metal-NP–PS is a parasitic effect since it can lead to energy losses.[11] In the metal-NP–PS complex, the enhancement effect occurs mostly in the vicinity of the plasmon resonance whereas the semiconductor-based complex may show a strong enhancement in a wide-wavelength interval. Below, we again compare the properties of semiconductor-NP–PS and metal-NP–PS complexes.

Our model incorporates a photosystem I (PS I) and a single semiconductor NP, connected by a biolinker (Fig. 1). As photosystem, we choose the PS I reaction center (RC) from cyanobacteria (*Synechocystis* sp. PCC6803). This reaction center is one of the most studied photosystems in the current literature.[13–15] The reaction center contains 96 chlorophyll and 22 carotenoid molecules. All of these molecules are involved in light harvesting. Simultaneously, the central six chlorophylls take part in the electron-transfer process. The electron-transfer chain starts at the P700 chlorophyll molecules

---

[*] Prof. A. O. Govorov
Department of Physics and Astronomy
Ohio University
Athens, OH 45701 (USA)
E-mail: govorov@ohiou.edu

[**] The author thanks Itai Carmeli (Tel Aviv U.) and Sebastian Mackowski (Munich U.) for helpful discussions. This work was supported by the NSF and BioNanoTechnology Initiative at OU.

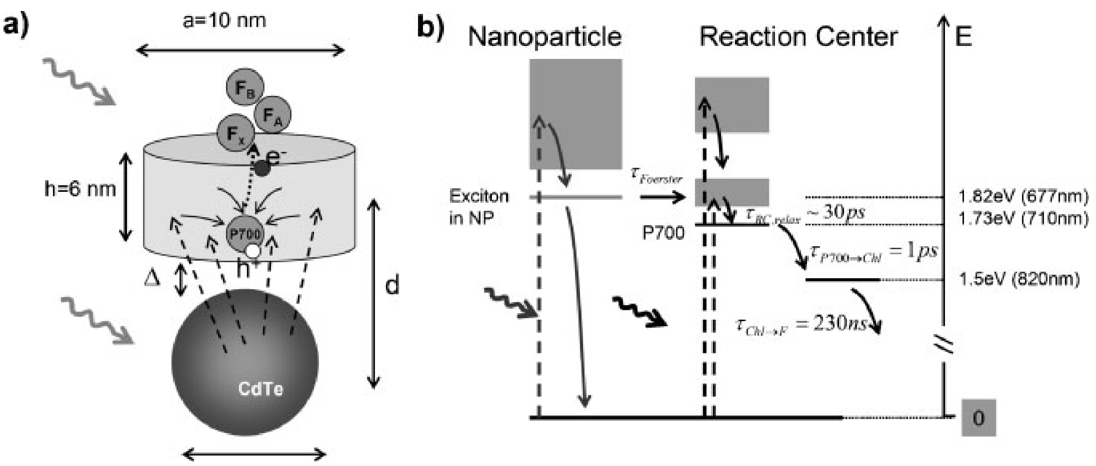

Figure 1. a) Geometry of the hybrid system. Förster energy transfer couples the CdTe nanoparticle and the reaction center. b) Schematic of physical processes. Arrows show the most important physical processes, including the NP-RC energy transfer, energy relaxation, and electron–hole separation.

(special pair or primary electron donor) and includes the primary acceptor chlorophylls, secondary acceptors, two phylloquinones, and three Fe_4S_4 clusters. We assume that the NP is bound to the RC from the electron donor side. In principle, a NP can be attached to both sides (acceptor or donor). In recent experiments, such conjugation has been realized using a sulfide bond with cysteine mutant in the protein.[4] In the light-harvesting process, an optically excited electron–hole pair becomes trapped at the spatial pair. Then, the special pair loses an electron, which travels across the membrane along the electron-transfer chain toward the Fe_4S_4 clusters. This electron transfer and sequential excitation of Fe_4S_4 clusters triggers a series of reactions, which eventually results in synthesis of ATP and reduction of $NADP^+$.[15]

The spatial structure of a RC of the PS I has been revealed by X-ray studies.[14] The dimensions of the RC are $10 \times 9\,\text{nm}^2$. The main body of chlorophyll molecules is found within a volume with dimensions $10 \times 6\,\text{nm}^2$. Therefore, we model an ensemble of absorbing chlorophylls as a cylinder of radius 5 nm and height 6 nm (Fig. 1a). The RC contains many chlorophyll molecules with different orientations of dipoles and absorbs photons coming from all directions. Therefore, we assume that absorption of light by "the chlorophyll cylinder" is isotropic. Figure 1b shows the diagram of flow of energy in the hybrid system. First, incident photons are absorbed by both the NP and RC. Excitons optically generated inside the NP can recombine inside the NP or can be transferred to the RC. The transfer process occurs via the FT mechanism. FT comes from the Coulomb interaction and does not require tunnel coupling between two objects. The excitation in the RC undergoes fast energy relaxation and ends up at the P700 special pair. The time of migration of excitation towards P700 inside the RC is $\tau_{\text{RC,relax}} \sim 30\,\text{ps}$. Once the excitation becomes trapped at the P700, the electron and hole are very efficiently separated, within $\tau_{P700 \to Chl} = 1\,\text{ps}$. In this process, the excited electron is transferred to the primary acceptor chlorophylls, whereas the hole remains trapped at the P700. A very high internal quantum yield of a PS I is guaranteed by very fast spatial separation of photo-generated electron and hole at the P700 special pair. The separation time $\tau_{P700 \to Chl}$ is much shorter than the typical recombination lifetimes in molecules ($\sim$1 ns). After electron transfer to the primary acceptor, the electron makes slower transitions and, in 230 ns, ends up in Fe_4S_4 clusters.[13] The above processes are unidirectional because they occur with loss of energy.

The absorption spectrum of the RC has two bands with wavelengths $\lambda_{\text{RC1}} \sim 680\,\text{nm}$ and $\lambda_{\text{RC2}} \sim 430\,\text{nm}$.[15] The 96 Chls inside the RC are responsible for the 680 nm band. The FT process is effective if the overlap between the emission spectrum of NP and the absorption spectrum of RC is significant. The absorption of optical energy inside the NP occurs if $\lambda < \lambda_{\text{exc}}$, where λ and λ_{exc} are the wavelengths of incident light and the exciton emission, respectively. Therefore, in order to assure efficient FT between NPs and RCs we should satisfy the condition: $\lambda_{\text{RC1}} \approx \lambda_{\text{exc}}$. Here we choose a spherical CdTe NP with a radius $R_{\text{NP}} = 4\,\text{nm}$. For this nanocrystal the corresponding exciton emission wavelength can be estimated as $\lambda_{\text{exc}} = 677\,\text{nm}$. This choice of NP parameters provides us with a strong overlap between the NP and RC spectra (Fig. 2). In the next step, we model the absorption spectrum of CdTe NP. In Ref. [17], it has been experimentally shown that the absorption cross section of colloidal NPs scales as $\propto R_{\text{NP}}^3$ if the wavelength of absorbed light is lower than λ_{exc}. This means that, for short wavelengths, we can neglect the quantization and use a dielectric model of NP to compute the absorption cross section. Strictly speaking, this approach is valid for the excitation energies: $E - E_{\text{exc}} > E_{\text{quant}}$, where E_{exc} and E_{quant} are the exciton and quantization energies, respectively. Within the simplified envelope-function method, $E_{quant} = \frac{\hbar^2\pi^2}{2\mu R_{NP}^2}$ and $E_{exc} = E_{g,CdTe} + E_{quant}$, where $\mu = 1/(m_e^{-1} + m_h^{-1})$ is the reduced effective mass of the exciton. We now consider a monochromatic electromagnetic wave that creates an electric field $\vec{e}E_0 \cos\omega t$ in the vicinity of the hybrid structure. The absorption rate of a spherical NP is

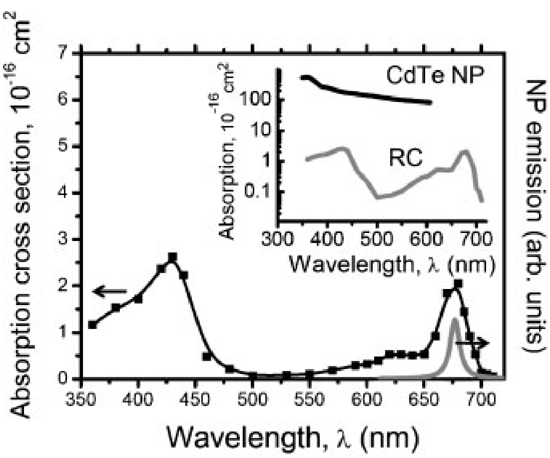

Figure 2. Absorption cross section of the reaction center [16] and the spectrum of exciton emission of the nanoparticle. Inset: Absorption cross sections for the reaction center and nanoparticle with a radius $R_{NP} = 4$ nm.

given by:

$$Q_{abs} = \frac{1}{2}\mathrm{Re}\int\limits_{V_{RC}} \vec{j}^{*}(r)\cdot\vec{E}(r)\,dV = \sigma_{NP} I_0, \qquad (1)$$

where $\varepsilon_{NP} = \varepsilon_{NP}(\omega)$ is the dynamic dielectric constant of CdTe, $\vec{E}(r) = \frac{3\varepsilon_0}{2\varepsilon_0+\varepsilon_{NP}}\vec{e}E_0 e^{-i\omega t}$ is the electric field inside the NP, $\vec{j}(r) = -i\omega\frac{\varepsilon_{NP}-1}{4\pi}\vec{E}(r)$ is the induced current, and ε_0 is the dielectric constant of a matrix. We choose $\varepsilon_0 = 1.8$, which corresponds to water and is also very close to the typical values for proteins ($n_0 = 1.33$). The incident light intensity and electric field are related through the equation $E_0^2 = \frac{8\pi I_0}{c\sqrt{\varepsilon_0}}$. The absorption cross-section of the NP can now be written as:

$$\sigma_{NP}(\omega) = V_{NP}\frac{\omega}{c\sqrt{\varepsilon_0}}\left|\frac{3\varepsilon_0}{2\varepsilon_0+\varepsilon_{NP}}\right|^2 \mathrm{Im}\varepsilon_{NP}, \qquad (2)$$

where $V_{NP} = 4\pi R_{NP}^3/3$ is the NP volume. In practice, Equation 2 provides us with a reliable estimate for $\lambda_{exc} - \lambda \leq 50\ nm$.[17] For example, the calculated cross section for a CdSe NP with $R_{NP} = 3.4$ nm at $\lambda = 500$ nm is 10×10^{-15} cm^2 and the corresponding experimental value obtained in Ref. [17] is 8.4×10^{-15} cm^2. In the inset of Figure 2, we compare the NP absorption cross section calculated for CdTe NP[18] with the absorption by RC. For the absorption cross section of the RC, we use the data from Ref. [16]. The results show that $\sigma_{NP} \gg \sigma_{RC}$; this inequality is rather typical for molecular and crystalline systems. This strongly suggests that we can take advantage by designing a hybrid system, in which the semiconductor component has a very large absorption cross section and the biomolecular component has an important functionality (such as efficient separation of electron–hole pairs in the RC).

In our model, the RC is approximated as an absorbing cylinder with a local isotropic conductivity $\beta_0(\omega)$. Inside the RC cylinder, the incident electromagnetic wave induces dissipative currents $\vec{j} = \beta_0(\omega)\vec{E}$. Then, we obtain from Equation 1:

$$\mathrm{Re}\beta_0 = \sigma_{RC}\frac{c\sqrt{\varepsilon_0}}{4\pi V_{RC}} \qquad (3)$$

where σ_{RC} is the absorption cross section of RC (see Fig. 2) and $V_{RC} = \pi a^2 h/4$ is the RC volume.

Exciton dynamics inside the hybrid structure is given by the standard rate equations:

$$\begin{aligned}\frac{\partial n_{NP}}{\partial t} &= \frac{\sigma_{NP} I_0}{\hbar\omega} - (\gamma_{NP}^0 + \gamma_{Foerster})n_{NP},\\ \frac{\partial n_{P700}}{\partial t} &= \frac{\sigma_{RC} I_0}{\hbar\omega} + \gamma_{Foerster} n_{NP} - \frac{n_{P700}}{\tau_{P700\to Chl}},\end{aligned} \qquad (4)$$

where n_{NP} and n_{P700} are the averaged numbers of excitons in a NP and at the P700 special pair; $\gamma_{NP}^0 = 1/\tau_{rec}^0$ and $\gamma_{\mathrm{Foerster}}$ are the intrinsic recombination rate of a NP and the rate of FT from a NP to a RC, respectively. Equation 4 assumes that the intra-RC relaxation time $\tau_{\mathrm{RC,relax}}$ is much shorter than the FT time. Indeed, $\tau_{\mathrm{RC,relax}} \sim 30$ ps and $1/\gamma_{\mathrm{Foerster}}$ will be found in the range of 40 ns. Owing to the inequality $\tau_{\mathrm{RC,relax}} \ll 1/\gamma_{\mathrm{Foerster}}$, the population of excited states of a RC does not enter Equation 4 explicitly. Under the stationary conditions ($\frac{\partial n_{NP}}{\partial t} = 0$ and $\frac{\partial n_{P700}}{\partial t} = 0$ the rate of generation of excited electrons in the electron-transfer chain calculated for the hybrid complex is given by:

$$R_{HS} = \frac{n_{P700}}{\tau_{P700\to Chl}} = \frac{I_0}{\hbar\omega}\left(\sigma_{RC} + \sigma_{NP}\frac{\gamma_{Foerster}}{(\gamma_{NP}^0 + \gamma_{Foerster})}\right) \qquad (5)$$

The rate $\gamma_{\mathrm{Foerster}}$ describes the strength of interaction between the NP and RC. A spherical CdTe NP has three optically active excitons with dipole moments along the *x*-, *y*-, and *z*-directions. Since the spin lifetime of an exciton in a NP at room temperature is short, populations of different types of excitons are almost the same. Therefore, the rate of FT in Equation 5 can be described as an average rate $\gamma_{\mathrm{Foerster}} = (\gamma_x + \gamma_{Fy} + \gamma_z)/3$, where γ_α is the rate of transfer for the exciton with a dipole moment along the α-axis ($\alpha = x,y,z$). A convenient formalism to calculate the FT rates for excitons in NPs is given in Refs. [19,20] This FT rate can be computed as

$$\begin{aligned}\gamma_\alpha &= \frac{2}{\hbar\omega}\mathrm{Re}\int\limits_{V_{RC}} \vec{j}^{\alpha}(r)\cdot\vec{E}^{\alpha *}(r)dV\\ &= \frac{2}{\hbar\omega}\sigma_{RC}(\omega_{exc})\frac{c\sqrt{\varepsilon_0}}{4\pi V_{RC}}\int\limits_{V_{RC}} \vec{E}^{\alpha}(r)\cdot\vec{E}^{\alpha *}(r)dV\end{aligned} \qquad (6)$$

where $\vec{E}^{\alpha}$ is the electric field induced by an oscillating dipole associated with the α-exciton; its field is given by is $\vec{E}_{\alpha}(r) = -\vec{\nabla}\frac{ed_{exc}(\vec{r}\cdot\vec{e}_{\alpha})}{\varepsilon_{eff}(x^2+y^2+z^2)^{3/2}}$, where $\vec{r}$ is the radius vector, d_{exc} is the magnitude of dipole moment, $\varepsilon_{eff} = (2\varepsilon_0 + \varepsilon_{CdTe})/3$, and $\vec{e}_{\alpha}$ is the unit vector along the dipole; for the dielectric constant of semiconductor, we take $\varepsilon_{\mathrm{CdTe}} = 7.2$. In Equation 6, the electric current is induced by the dipole field of exciton $\vec{j}^{\alpha} = \beta_0(\omega)\vec{E}^{\alpha}$. In addition, from simple algebra, we obtain $\sum_{\alpha=x,y,z}\vec{E}^{\alpha}(r)\cdot\vec{E}^{\alpha*}(r)/3 = 2/r^6$.

Equation 6 was written under the assumption that the exciton in a NP has a definite energy. In reality, the exciton peak is broadened, which results in a replacement in Equation 6:

$$\sigma_{RC} \rightarrow \overline{\sigma}_{RC} = \int_{\omega_{\min}}^{\omega_{\max}} F(\omega)\sigma_{RC}(\omega)d\omega \tag{7}$$

where the function $F(\omega)$ describes the normalized absorption of a donor (i.e., a NP) in the FT process: $F(\omega) = \frac{1}{\pi}\frac{\Delta\omega}{(\omega-\omega_{exc})^2+\Delta\omega^2}$. For the exciton broadening of a NP, we take a typical number $\Delta\omega = 27$ meV that corresponds to the FWHM $2\Delta\lambda = 20$ nm. For the limits in the integral, we chose: $\omega_{\min(\max)} = 1.73$ eV(2.30 eV). The resultant FT rate takes the form

$$\gamma_{Foerster} = \overline{\sigma}_{RC}\frac{c\sqrt{\varepsilon_0}}{\hbar\omega\pi}\left(\frac{ed_{exc}}{\varepsilon_{eff}}\right)^2\frac{1}{d^6}A, \tag{8}$$

where d is the NP-RC center-to-center distance and $A = \frac{d^6}{V_{RC}}\int_{V_{RC}}\frac{1}{r^6}dV$ is a geometrical factor. The exciton dipole can be estimated from a typical exciton lifetime of CdTe NPs. We obtain $d_{\mathrm{exc}} = 0.2$ nm, assuming $\tau^0_{rec} \approx 20$ ns and the quantum yield $Y_{\mathrm{NP}} = 1$. With the geometrical parameters $a = 10$, $h = 6$, $R_{\mathrm{NP}} = 4$, and $\Delta = 1$ nm, the calculated geometrical factor is $A = 1.3$. The resultant FT rate $\gamma_{\mathrm{Foerster}} = 2.5 \times 10^7\ \mathrm{s}^{-1}$. This number implies that the time of energy transfer ($\tau_{Foerster} = 1/\gamma_{Foerster}$) is longer than the exciton recombination time of NP: $\tau_{Foerster}/\tau^0_{rec} \approx 2$. In Figure 3, we show the rates of generation of excited electrons for the hybrid NP–RC system (R_{HS}) and for the RC alone (R_{RC}). The rate R_{HS} was calculated from Equation 4 and $R_{RC} = I_0\sigma_{RC}/\hbar\omega$. We see very strong increase of the rate R_{HS} compared to R_{RC}. Interestingly, this happens despite the fact that $\frac{\gamma_{Foerster}}{(\gamma^0_{NP}+\gamma_{Foerster})} \sim 0.33 < 1$. The physical reason for the strong enhancement in the hybrid system is the strongly enhanced absorption in a CdTe NP. We also note that Equation 8 takes into account FT from a NP to the surface of the RC. For the chosen parameters, NP-surface transfer leads to a slightly increased geometrical factor ($A = 1.3$). For small exciton-surface distances ($R_{\mathrm{NP}} + \Delta$), the geometrical factor A becomes a large number.

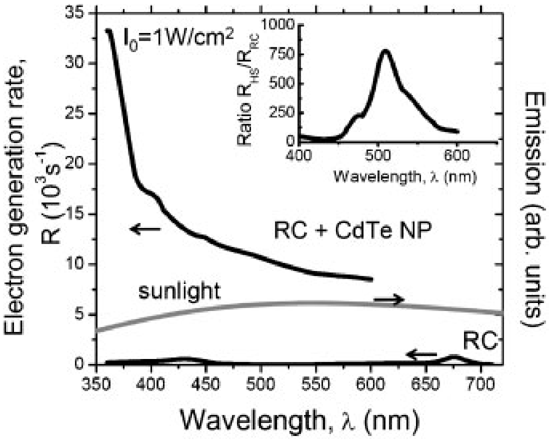

Figure 3. Calculated rates of generation of excited electrons for the RC alone and for the hybrid RC–NP system. The light intensity is $I = 1\ W/cm^2$. The red curve gives the spectral energy density of sunlight radiation as a function of wavelength, $U_{\lambda} \propto \lambda^{-5}/(e^{\frac{2\pi\cdot\hbar c}{\lambda\cdot k_B T}} - 1)$. Inset: The ratio of the rates for the RC and hybrid complex.

We now can evaluate the ratio of the total absorption of sunlight for the systems. The sunlight spectrum is close to the spectrum of a black body at $T_{\mathrm{s}} = 5200$ K, $U_{\omega} \propto \omega^3/(e^{\frac{\hbar\omega}{k_B T_s}} - 1)$ (see Fig. 3). The total rate of electron generation within a given photon-energy interval is given by: $R_{tot,HS} = \int_{\omega_1}^{\omega_2} U_{\omega}\cdot R_{HS}(\omega)d\omega$. Using Equation 5 and the experimental data for $R_{\mathrm{HS}}(\omega)$, we obtain: $R_{tot,HS}/R_{tot,RC} \approx 77$. For the limits of integration, we assumed $\hbar\omega_{1(2)} = 2.05$ eV(3.42 eV) that corresponds to $\lambda_{1(2)} = 360$ nm(600 nm). Within the above interval, the cross section of the NP is well-approximated by Equation 2. In principle, the hybrid NP–RC complex can harvest light energy in the interval $\hbar\omega > \hbar\omega_{exc} = 1.82$ eV or $\lambda < \lambda_{\mathrm{exc}} = 677$ nm. The ratio $R_{tot,HS}/R_{tot,RC}$ strongly depends on the distance between the RC and NP and rapidly decreases with the biolinker length Δ (Fig. 4).

We should also comment on the quantum yield of the hybrid complex, defined as $Y_{HS} = \frac{R_{HS}}{R_{abs}}$, where $R_{abs} = \frac{I_0}{\hbar\omega}(\sigma_{RC} + \sigma_{NP})$ is the total rate of photon absorption by the hybrid system. As mentioned above, due to the very short relaxation times ($\tau_{RC,relax} \sim 30$ ps and $\tau_{P700\rightarrow Chl} = 1$ ps), the RC itself has a very high quantum yield $Y_{\mathrm{RC}} \approx 1$. Therefore, main losses in the hybrid system come from recombination of excitons in a NP and the yield becomes $Y_{HS} \approx \frac{\gamma_{Foerster}}{(\gamma^0_{NP}+\gamma_{Foerster})}$; the above equation was obtained under the conditions $\sigma_{\mathrm{NP}} \gg \sigma_{\mathrm{RC}}$ and $\gamma^0_{NP} \sim \gamma_{Foerster}$. We can see that the resultant quantum yield becomes relatively low: $Y_{\mathrm{HS}} \approx 0.33$ for the bio-linker with $\Delta = 1$ nm. However, the total rate of production of electrons strongly increased: $R_{tot,HS}/R_{tot,HS} \approx 77$. Basically, the reduced quantum yield is a "price" for the strongly enhanced absorption.

In the final part of this Communication, we discuss advantages and disadvantages of hybrid semiconductor-NP–PS

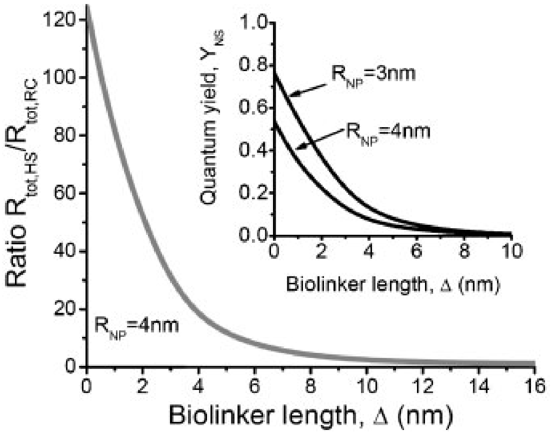

Figure 4. Calculated ratios of integrated rates for the RC and for the hybrid RC–NP system as a function of the biolinker length. Inset: Quantum yields for the RC and hybrid complex as functions of the biolinker length.

molecule structures. The quantum yield strongly depends on the geometry of the system. For example, for the same NP with $R_{\rm NP} = 4$ nm, the calculated yield strongly increases if we decrease the distance to the RC: $Y_{\rm HS} \approx 0.54$ for $\Delta = 0$. Another way to increase $Y_{\rm HS}$ is to decrease the NP radius (inset of Fig. 4). But, in this case, we also decrease the absorption by a NP and therefore $R_{\rm HS}$ decreases. However, few or several smaller NPs can be attached to one RC and, in this way, $R_{\rm HS}$ can be increased keeping a decent value of $Y_{\rm HS}$. For example, $Y_{\rm HS} \approx 0.53$ if we choose $R_{\rm NP} = 3$ nm, $\Delta = 1$ nm, and the geometry shown in Figure 1. The geometry convenient for photocurrent experiments is shown in Figure 5, it resembles the system studied experimentally in Ref. [3]. In the structure shown in Figure 5, a photogenerated electron and hole become first separated inside the RC and then forwarded to the conducting contacts. The resultant photocurrent is proportional to $R_{\rm HS}$. The role of semiconductor NPs in this structure is to enhance the absorption cross section and to supply excitons to the RC. The role of RC is to rapidly separate the electron and hole. The structure in Figure 5 includes three NPs and a RC. In particular, excitons generated in the NP1 are channeled to the RC via the NP2. The NPs 1 and 2 communicate via the FT mechanism. The NPs 2 and 3 are coupled with the RC again via the FT process. The rate of generation of excitons is where $\gamma_{Foerste,NP1\rightarrow NP2}$ is the rate for the FT process NP1 → NP2. For simplicity, we assume that all NPs have the same γ^0_{NP}. A similar cascade transfer was studied theoretically and realized in Ref. [21]. The rate of FT between NPs can be

$$R_{HS} = \frac{I_0}{\hbar\omega}\left(\sigma_{RC} + 2\sigma_{NP2}\frac{\gamma_{Foerster,NP2\rightarrow RC}}{(\gamma^0_{NP} + \gamma_{Foerster,NP2\rightarrow RC})} + \sigma_{NP1}\frac{\gamma_{Foerster,NP1\rightarrow NP2}}{(\gamma^0_{NP} + \gamma_{Foerster,NP2\rightarrow NP2})}\frac{\gamma_{Foerster,NP2\rightarrow RC}}{(\gamma^0_{NP} + \gamma_{Foerster,NP2\rightarrow RC})}\right) \tag{9}$$

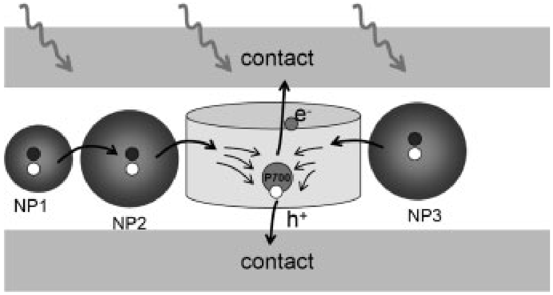

Figure 5. Geometry for photocurrent experiments. The FT mechanism couples three semiconductor NPs and a RC.

estimated by

$$\gamma_{Foerster,NP1\rightarrow NP2} \approx \frac{V_{NP2}}{\pi\hbar}\left(\frac{ed_{exc}}{\varepsilon_{eff}}\right)^2\left|\frac{3\varepsilon_0}{2\varepsilon_0 + \varepsilon_{NP}(\omega_{exc,NP2})}\right|^2\frac{1}{d^6}{\rm Im}\varepsilon_{NP}(\omega_{exc,NP2}) \tag{10}$$

where d is the center-to-center distance between NPs and $\omega_{exc,NP2}$ is the frequency of NP2. We now assume the following parameters: $R_{NP1} = 3$ nm, $R_{NP2} = 4$ nm, $\Delta_{NP1-NP2} = \Delta_{NP2-RC} = 1$ nm, where $\Delta_{NP1-NP2(NP2-RC)}$ are the surface-to-surface spatial separations. The calculated FT rates are: $\gamma_{Foerster,NP1\rightarrow NP1}/\gamma^0_{NP} = 17$ and $\gamma_{Foerster,NP2\rightarrow RC}/\gamma^0_{NP} = 0.29$. We see that the slowest step is the process NP2 → RC. The step NP1 → NP2 is fast ($1/\gamma_{Foerster,NP1\rightarrow NP1} \sim 1.2$ ns) and does not lead to significant losses of energy. For the structure in Figure 5, the quantum yield $Y_{\rm HS} \approx 0.37$. For the same structure and wavelength interval $360\,{\rm nm} < \lambda < 550\,{\rm nm}$, we obtain $R_{tot,HS}/R_{tot,RS} \approx 115$.

The hybrid structure proposed here has a strongly increased rate of generation of electrons because the absorption cross section of a semiconductor NP is much larger than that of a RC. Simultaneously, the interaction between a NP and RC via Förster transfer is the central mechanism resulting in enhanced opto-electronic properties. A NP in the hybrid structure delivers excitons to a RC where they become separated within a very short time. A disadvantage of the hybrid structure is that the quantum yield becomes reduced. This happens owing to recombination of excitons in a NP. Our modeling shows that excitons of a NP have a chance to recombine since the time of FT from a NP to a RC is relatively long. The reasons for the relatively long time for the process NP → RC are the following: (1) The absorption cross section of a RC is not very large, and (2) the NP–RC center-to-center distance is relatively long since it is dictated by the size of the RC. In order to increase the quantum yield of a hybrid structure, one should decrease the effective distance between NP and RC. For example, one can use NPs with smaller sizes or shorter biolinkers. Possible ways to increase the rate of production of electrons are illustrated in Figure 5. To obtain an enhanced rate $R_{\rm HS}$, one can use few or several NPs attached to a RC or one can assemble chains of

NPs with cascade energy transfer. For light-harvesting applications, the hybrid structure proposed here has a strong advantage if we deal with one monolayer or a thin film. The amount of light energy absorbed by a thin film composed of hybrid complexes will be greatly enhanced. However, if we study a thick film, a reduced quantum yield may be a limiting factor and we should look at the total external quantum yield. It is also interesting to compare our hybrid system with the structure composed of metal NPs and chlorophylls.[11,12] The metal–chlorophyll complexes have strongly enhanced absorption owing to the plasmon resonance in a metal NP. Compared to the semiconductor-based complex, the metal–photosystem complex has some disadvantages. (1) A metal-based structure has strong absorption by a metal NP and, therefore, a low quantum yield. We should note that an absorption cross section of metal NP is typically much greater than that of semiconductor. (2) Enhancement occurs only in the vicinity of the plasmon frequency. In the semiconductor-based complex, the enhancement effect is expected in the wide interval $\lambda < \lambda_{\text{exc}}$.

The natural photosynthesis systems typically include both reaction centers and antenna chlorophylls. These components (RC and antenna chlorophylls) are built into a membrane that holds the system components. The antenna chlorophylls serve to absorb photons and to deliver them to the reaction center via the FT mechanism. In the system with reaction centers and antenna chlorophylls, the enhancement effect can also be archived by attaching semiconductor NPs to the antennas. Experimentally, NPs can be attached to a membrane that contains photosystems and the enhancement effect can be observed as an increased rate of production of a chemical “fuel” (e.g., ATP molecules).

To conclude, natural photosystems absorb light mostly within certain wavelength intervals. A hybrid structure composed of a photosystem and semiconductor nanoparticles can efficiently harvest light energy in a much wider wavelength interval. Moreover, the rate of production of excited electrons by the hybrid structure is strongly enhanced compared to the photosystem alone. Geometry of hybrid structure plays the crucial role. For certain organizations of hybrid complexes, the enhancement factor can be up to 100.

Received: December 2, 2007
Revised: January 7, 2008

[1] M. Bruchez, Jr., M. Moronne, P. Gin, S. Weiss, P. A. Alivisatos, *Science* **1998**, *281*, 2013.

[2] W. C. W. Chan, S. Nie, *Science* **1998**, *281*, 2016.

[3] R. Das, P. J. Kiley, M. Segal, J. Norville, A. A. Yu, L. Wang, A. S. Trammell, L. E. Reddick, R. Kumar, F. Stellacci, N. Lebedev, J. Schnur, B. D. Bruce, S. Zhang, M. Baldo, *Nano Lett.* **2004**, *4*, 1079.

[4] L. Frolov, Y. Rosenwaks, C. Carmeli, I. Carmeli, *Adv. Mater.* **2005**, *17*, 2434.

[5] I. L. Medintz, H. T. Uyeda, E. R. Golgman, H. Mattoussi, *Nat. Mater.* **2005**, *4*, 435.

[6] R. C. Somers, M. G. Bawendi, D. G. Nocera, *Chem. Soc. Rev.* **2007**, *36*, 579.

[7] C. D. Geddes, J. R. Lakowicz, *J. Fluorescence* **2002**, *12*, 121.

[8] P. Anger, P. Bharadwaj, L. Novotny, *Phys. Rev. Lett.* **2006**, *96*, 113002.

[9] J. Lee, P. Hernandez, J. Lee, A. O. Govorov, N. A. Kotov, *Nat. Mater.* **2007**, *6*, 291.

[10] I. Carmeli, B. Zebli, L. Frolov, C. Carmeli, S. Richter, A. W. Holleitner, *Adv. Mater.* **2007**, *19*, 3901.

[11] A. O. Govorov, I. Carmeli, *Nano Lett.* **2007**, *7*, 620.

[12] S. Mackowski, S. Wörmke, A. J. Maier, T. H. P. Brotosudarmo, H. Harutyunyan, A. Hartschuh, A. O. Govorov, H. Scheer, C. Bräuchle, *Nano Lett.* **2008**, *8*, 558.

[13] K. Brettel, W. Leibl, *Biochim. Biophys. Acta* **2001**, *1507*, 100.

[14] N. Krauss, W. Hinrichs, I. Witt, P. Fromme, W. Pritzkow, Z. Dauter, C. Betzel, K. S. Wilson, H. T. Witt, W. Saenger, *Nature* **1993**, *361*, 326.

[15] M. Yang, A. Damjanovic, H. M. Vaswani, G. R. Fleming, *Biophys. J.* **2003**, *85*, 140.

[16] I. Carmeli, C. Carmeli, unpublished.

[17] C. A. Leatherdale, W.-K. Woo, F. V. Mikulec, M. G. Bawendi, *J. Phys. Chem. B* **2002**, *106*, 7619.

[18] E. D. Palik, *Handbook of Optical Constants of Solids*, Academic, New York **1985**.

[19] A. O. Govorov, G. W. Bryant, W. Zhang, T. Skeini, J. Lee, N. A. Kotov, J. M. Slocik, R. R. Naik, *Nano Lett.* **2006**, *6*, 984.

[20] A. O. Govorov, J. Lee, N. A. Kotov, *Phys. Rev. B* **2007**, *76*, 125308.

[21] J. Lee, A. O. Govorov, N. A. Kotov, *Nano Lett.* **2005**, *5*, 2063.